

# Entanglement Harvesting with Moving Mirrors in (1+1) Dimensions

Wan Cong,<sup>1,2,\*</sup> Erickson Tjoa,<sup>1,2,†</sup> and Robert B. Mann<sup>1,2,‡</sup>

<sup>1</sup>*Department of Physics and Astronomy, University of Waterloo, Waterloo, Ontario, N2L 3G1, Canada*

<sup>2</sup>*Institute for Quantum Computing, University of Waterloo, Waterloo, Ontario, N2L 3G1, Canada*

(Dated: November 25, 2021)

We study the phenomenon of entanglement extraction from the vacuum of a massless scalar field in  $(1+1)$  dimensional spacetime in presence of a moving Dirichlet boundary condition, i.e. *mirror spacetime*, using two inertial Unruh-DeWitt detectors. We consider a variety of non-trivial trajectories for these accelerating mirrors and find (1) an entanglement inhibition phenomenon similar to that recently seen for black holes, providing another connection between Hawking radiation and the dynamical Casimir effect, as well as (2) trajectory-independent entanglement enhancement in some regimes. We clarify the role of the infrared ambiguity in both the response function of a detector and the concurrence of two detectors.

## I. INTRODUCTION

The study of quantum entanglement has far-reaching consequences in many fields, such as in the study of black hole entropy [1, 2] and the anti-de Sitter/conformal field theory (AdS/CFT) correspondence [3]. In more formal algebraic quantum field theory, it was shown that the vacuum state of a quantum field can maximally violate Bell's inequalities [4]. A more operational approach to study quantum field entanglement was initiated in [5], where it was shown that atoms initialized as uncorrelated states can become entangled after some time due to the global nature of field correlators. This particle detector model, now known as the Unruh-DeWitt (UDW) model, has been extensively used to study the phenomenon of entanglement harvesting [6, 7], discerning the topology of spacetime [8] and distinguishing a thermal bath from an expanding universe at the same temperature [9], among others. This operational approach has the advantage that it is easy to apply even in curved spacetimes.

Here we study the phenomenon of entanglement harvesting in the context of *mirror spacetimes* i.e. the Minkowski spacetime spatially divided by a (possibly dynamical) Dirichlet boundary condition, in  $(1+1)$  dimensions. This would constitute the first investigation of entanglement harvesting in a highly non-stationary background quantum field essentially due to the Dynamical Casimir effect (DCE). The DCE has been recently observed experimentally [10] thus motivating the use of mirror spacetimes to study aspects of particle creation in quantum field theory.

The conformal invariance of the massless wave equation in  $(1+1)$  dimensions, together with the ease of obtaining exact analytic expressions for the Wightman functions of moving mirrors in certain classes of trajectories, make the study of mirror spacetimes a very attractive toy model to gain insights into the physics of quantum fields in curved spacetimes. The study of responses

and transition rates of UdW detectors in receding mirror spacetimes was first investigated decades ago [11–13]. For some classes of trajectories, one can even match certain mirror trajectories to Hawking radiation associated with black hole spacetimes, whether at the level of the response rate [14] or at the level of the Bogoliubov transformation and stress-energy tensor [15]. More recently it has been shown that for some generic trajectories certain limits can also be taken to obtain thermal responses [16] or even model black hole collapse from a null shell [17–19]. We note in this context that a study of entanglement harvesting in black hole spacetimes was recently initiated for the first time for  $(2+1)$ -dimensional black holes [20], and so it is of further interest to investigate entanglement harvesting in spacetimes with non-trivial boundary conditions that could simulate the collapse of matter into a black hole.

We will see that, despite the differences between the physics of mirrors and black holes, a pair of atoms can experience (1) entanglement inhibition and even *entanglement death* near a mirror, an effect also associated with the event horizon of a black hole [20], as well as (2) trajectory-independent entanglement enhancement in some regimes. We also clarify the role of the infrared (IR) ambiguity for massless fields in  $(1+1)$  dimensions and explain how entanglement measures do not suffer the same ambiguity issue that plagues calculations of response functions. Furthermore, we clarify the fact that the regularity of the concurrence can be used to induce a natural IR cutoff for the free-space Wightman function, a result we believe is slightly underappreciated.

Our paper is organized as follows. In section II we describe the setup involving the UDW model and provide several *ray-tracing functions* for the mirror trajectories that will be studied in this paper. In section III A we study entanglement harvesting between two detectors in the presence of a static mirror and also a non-inertial mirror first studied in [15]. In section III C we compare these results with that of a mirror trajectory recently described in [21] that mimics the null black hole collapse model. In section III D we clarify the effect of having a Dirichlet boundary condition on transition probability and concurrence in the ‘far-from-mirror’ limit, before

\* wcong@uwaterloo.ca

† e2tjoa@uwaterloo.ca

‡ rbmann@uwaterloo.ca

finally concluding in section IV.

In this paper we adopt the natural units  $c = \hbar = 1$ .

## II. SETUP

In this section we recall the standard UDW model in the context of a massless scalar field in (1+1) dimensions interacting with a first quantized atom. In the Dirac picture, the light-matter interaction is provided by the interacting Hamiltonian of the form

$$H_I^j = \lambda \chi_j(t) \hat{\mu}_j(t) \otimes \hat{\phi}(\mathbf{x}_j(t)), \quad j = A, B \quad (1)$$

where  $\lambda$  is the coupling strength<sup>1</sup>,  $\chi(t)$  is a switching function,  $\hat{\phi}$  is the field operator and  $\mathbf{x}_j(t) = (t, x_j(t))$  is the trajectory of the atomic detector. In addition,  $\hat{\mu}_j(t) = \hat{\sigma}_j^+ e^{i\Omega_j t} + \hat{\sigma}_j^- e^{-i\Omega_j t}$  is the monopole moment of the detector, where  $\sigma^\pm$  are the ladder operators of the  $\mathfrak{su}(2)$  algebra and  $\Omega_j$  is the energy gap of the two-level atom. The index  $j = A, B$  indicates which atom (UDW detector) we are considering: in the case of entanglement harvesting, we have two atomic detectors so the full interacting Hamiltonian takes the form

$$H_I = H_I^A \otimes I_B + I_A \otimes H_I^B. \quad (2)$$

We shall also consider for simplicity the case where the two atoms are identical so  $\Omega = \Omega_A = \Omega_B$ . The time

parameter  $t$  is the proper time of both detectors, which is the same since we consider both atoms to be at rest relative to each other. We do not consider them in relative motion in order to not mix the effect of this relative motion with the contributions due to the moving mirror.

We consider the initial state of the full system to be a separable state  $\rho_0 = |\psi\rangle\langle\psi|$  where  $|\psi\rangle = |0\rangle|g\rangle_A|g\rangle_B$ , and where  $|0\rangle$  is the field vacuum and  $|g\rangle$  is the atomic ground state. The final state of the detector  $\rho_{AB}$  is obtained by tracing out the field state after time evolution:

$$|\psi_f\rangle = \mathcal{T} \exp\left(-i \int dt H_I(t)\right) |\psi\rangle := \hat{U} |\psi\rangle, \quad (3)$$

$$\rho_{AB} = \text{Tr}_\phi |\psi_f\rangle\langle\psi_f|. \quad (3)$$

In the  $\{|g\rangle, |e\rangle\}$  basis, the joint state of the detectors will be given by the matrix [8]

$$\rho_{AB} = \begin{pmatrix} 1 - P_A - P_B & 0 & 0 & X^* \\ 0 & P_B & C & 0 \\ 0 & C^* & P_A & 0 \\ X & 0 & 0 & 0 \end{pmatrix} + O(\lambda^4). \quad (4)$$

The expressions for  $X, P_j$  (we are not using  $C$  in this paper) are given by

$$X = -\lambda^2 \iint dt dt' \chi_A(t) \chi_B(t') e^{-i\Omega(t+t')} \left[ \Theta(t' - t) W(\mathbf{x}_A(t), \mathbf{x}_B(t')) + \Theta(t - t') W(\mathbf{x}_B(t'), \mathbf{x}_A(t)) \right], \quad (5)$$

$$P_j = \lambda^2 \iint dt dt' \chi_j(t) \chi_j(t') e^{-i\Omega(t-t')} W(\mathbf{x}_j(t), \mathbf{x}_j(t')) \quad (6)$$

where  $W(\mathbf{x}, \mathbf{x}') = \langle 0 | \hat{\phi}(\mathbf{x}) \hat{\phi}(\mathbf{x}') | 0 \rangle$  is the pullback of the Wightman function to the detector trajectories and  $\Theta(\cdot)$  is the Heaviside step function. Since the detectors are identical, we also choose the same Gaussian switching function  $\chi(t)$  for both detectors,

$$\chi_j(t) = \exp\left[-\frac{(t - t_j)^2}{2\sigma^2}\right] \quad (7)$$

where the parameter  $\sigma$  characterises the length of the switching and hence the duration of interaction with the field and  $t_j$  is the temporal peak of the switching.

The entanglement measure we use here is concurrence  $\mathcal{C}(\rho_{AB})$ , computed in this case to be [8]

$$\mathcal{C}(\rho_{AB}) = 2 \max\left\{0, |X| - \sqrt{P_A P_B}\right\} + O(\lambda^4) \quad (8)$$

which is simple and transparent for our purposes<sup>2</sup>.

In (1+1) dimensions, the metric for Minkowski space-time can be written in terms of double null coordinates  $u, v = t \mp x$  so that

$$ds^2 = dt^2 - dx^2 = du dv. \quad (9)$$

<sup>1</sup> Note that in (1+1) dimensions, the coupling constant is not dimensionless but has units of inverse length in natural units. Here we say that a small coupling constant means the dimensionless quantity  $\lambda\sigma$  is small, where  $\sigma$  is the width of the Gaussian switching function.

<sup>2</sup> Negativity  $\mathcal{N}$  is another usable well-known entanglement measure but in this context does not yield qualitatively different results; furthermore concurrence admits a simpler interpretation due to a clean separation of local and nonlocal terms.

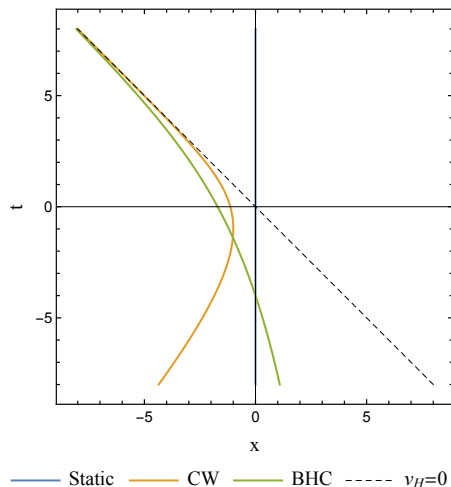


FIG. 1. The various mirror trajectories considered in this paper are shown here, with  $\kappa = 0$  for CW and  $\kappa = 1/4$  and  $v_H = 0$  for BHC.

The Wightman function for massless scalar field in  $(1+1)$  dimensions in terms of these coordinates is

$$W_f(x, x') = -\frac{1}{4\pi} \log \left[ \Lambda^2 (\epsilon + i\Delta u)(\epsilon + i\Delta v) \right] \quad (10)$$

where the logarithm is taken with respect to the principal branch, the subscript  $f$  denotes ‘free space’,  $\Lambda$  is an IR cutoff and  $\epsilon$  is a UV cutoff. In free space, the IR regulator cannot be removed, which is a peculiarity of  $(1+1)$  dimensions alone [22]. This leads to the well-known IR ambiguity in the response of a detector coupled linearly to  $(1+1)$  massless scalar field.

The presence of a mirror, i.e. a (moving) Dirichlet boundary condition, removes this IR ambiguity via the “method of images”. It modifies the Wightman function via *ray-tracing functions*  $p(u)$  or  $f(v)$  depending on whether we use  $u$  or  $v$  to ‘trace’ rays: in the presence of a mirror, some of the ‘reflected’ right-moving modes can be written in terms of the incoming left-moving modes. Anticipating our results, we choose  $p(u)$  to avoid issues involving coordinate singularities (see e.g. [15] or [16]) and the Wightman function is now given by [11]

$$W(x, x') = -\frac{1}{4\pi} \log \left[ \frac{(\epsilon + i(p(u) - p(u')))(\epsilon + i(v - v'))}{(\epsilon + i(p(u) - v'))(\epsilon + i(v - p(u')))} \right] \quad (11)$$

For a static mirror located at the origin  $x = 0$  we have  $p(u) = u$ , and the result reduces to the well known fact that the Wightman function is the difference between the free-space Wightman function and its parity-reversed counterpart [14].

In this paper we will consider three ray-tracing func-

tions, corresponding to three different trajectories [16]:

$$\begin{aligned} p_0(u) &= u, \\ p_1(u) &= -\frac{1}{\kappa} e^{-\kappa u}, \\ p_2(u) &= v_H - \frac{1}{\kappa} W \left( e^{-\kappa(u-v_H)} \right) \end{aligned} \quad (12)$$

where  $W(x)$  is the Lambert  $W$ -function. The corresponding trajectories are shown in Figure 1.

The ray-tracing function  $p_0$  describes a static mirror located at the origin. The function  $p_1$  corresponds to a mirror that emits thermal radiation just like that of an eternal black hole, and is known as the *Carlitz-Willey* (CW) trajectory [15]. We shall call the last ray-tracing function  $p_2$  the *black hole collapse* (BHC) trajectory, since it has been shown that there is one-to-one correspondence between the Bogoliubov coefficients for this moving mirror setup and the scenario of  $(1+1)$  null shockwave collapse [17, 21, 23]. In both cases the parameter  $\kappa$  can be interpreted as some kind of acceleration parameter since both  $p_1, p_2$  correspond to non-inertial motion of the mirror.

We focus on these functions because they are regular for all  $u \in \mathbb{R}$ . Both  $p_1, p_2$ , have future horizons; hence the corresponding ray tracing function in terms of  $v$  will be singular at some finite  $v$ . However they have no past horizons and  $p(u)$  is fully regular. By contrast, a mirror that follows an eternal Rindler trajectory will have both past and future horizons, which can lead to technical difficulties in evaluating the entries in the reduced density matrix  $\rho_{AB}$  due to a coordinate singularity in the ray-tracing function. Despite modelling collapse, the BHC trajectory has a regular ray-tracing function because the Lambert  $W$ -function (also known as the product-log function)  $W(z)$  is a well-defined injective function, since  $z \geq 0$  for  $u \in \mathbb{R}$ .

In this paper, we shall study entanglement harvesting primarily using numerical means, since we do not have the usual advantage of stationarity of the Wightman function: our setups, except in the static mirror scenario, are not time-translation invariant due to the non-constant proper acceleration of the mirror. This is true even in the simple case of two static detectors relative to lab frame coordinates  $(t, x)$  (again, except when the mirror itself is static).

For all of our results, we verify numerically convergence in the parameter  $\epsilon$  in (11). The cut-off value is chosen such that the error due to the finite value of  $\epsilon$  is  $\leq 10^{-4}$  which is smaller than the precision of the numerical results presented. There are instances when choosing very small  $\epsilon \lesssim 10^{-9}$  is *essential* for numerical stability, while at other times  $\epsilon \lesssim 10^{-6}$ , for instance, may be sufficient.

### III. RESULTS AND DISCUSSIONS

We will first consider the case of a static mirror and a CW mirror since they cover the generic features that we wish to understand.

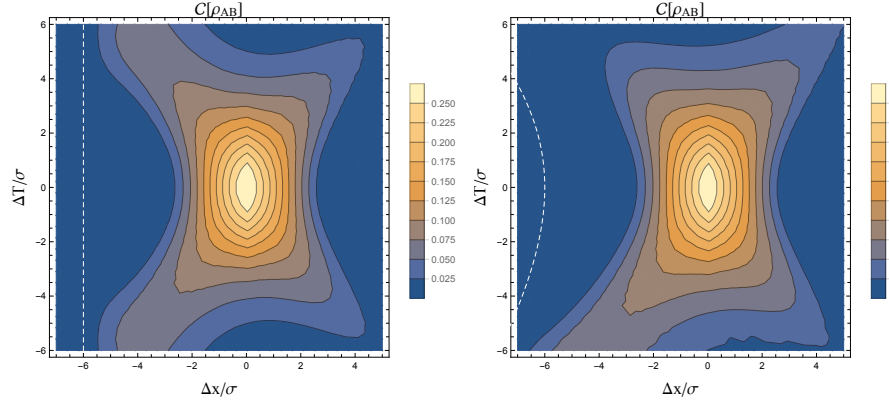


FIG. 2. Comparing entanglement harvesting near a static and a CW mirror, centered at detector  $A$ , which is located at the origin. **Left:** Static mirror,  $d_A/\sigma = 6$ . **Right:** CW mirror,  $d_A/\sigma = 6$  and  $\kappa\sigma = 0.25$ . The entanglement profiles are sensitive to the trajectories of the mirrors, though the sensitivity drops as the detectors move further from the mirror, as shown in Figure 3. In these plots,  $\Omega\sigma = 1$ .

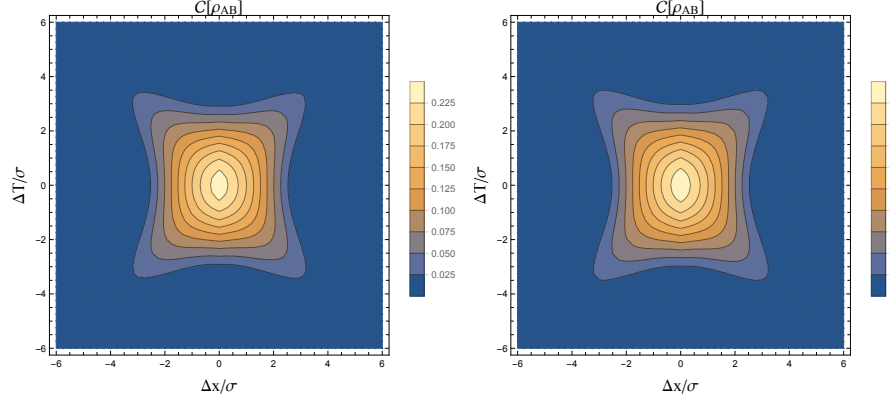


FIG. 3. Concurrence contour plots for spacetime region centered at detector  $A$ , which is located at the origin in these figures. **Left:** Concurrence in free space (with no mirror), with the IR cutoff set at  $\Lambda = 10^{-3}$ . **Right:** Concurrence in the presence of a static mirror, with the mirror located far from detector  $A$  at  $d_A/\sigma = 400$ . In these plots,  $\Omega\sigma = 1$ .

### A. Static Mirrors

We are interested in understanding how the presence of a reflective boundary will affect the amount of entanglement harvested between different spacetime points as compared to the corresponding free space situation. For this purpose, we fix detector  $A$  at specific spacetime points, and look at how the amount of entanglement harvested changes when detector  $B$  is moved to various spacetime positions relative to  $A$ , generalizing a recent study for two static detectors in the absence of a mirror or any Dirichlet boundary condition [7].

These results are shown in Figures 2, 3, and 4. We let  $(t_A, x_A)$  ( $(t_B, x_B)$ ) denote the spacetime position of  $A$  ( $B$ ) where  $t_A$  ( $t_B$ ) is the peak of the Gaussian switching. In these figures, the vertical axes correspond to the time delay  $\Delta T = t_B - t_A$  and the horizontal axes to separation between the detectors,  $\Delta x \equiv x_B - x_A$ , where concurrence  $\mathcal{C}[\rho_{AB}]$  is plotted as a function of  $(\Delta T, \Delta x)$ . The coloured regions correspond to values of  $\mathcal{C}[\rho_{AB}]$  between the de-

tectors that are bounded between the contours, which denote lines of constant concurrence.

The mirror trajectories are shown as dashed white curves. As the mirrors are not static, the distance between the mirror and the detectors can vary in time. Nonetheless, we shall use  $d_A$ , the instantaneous proper distance between  $A$  and the mirror at the time  $t_A$  (peak of Gaussian switching), as an indication of how far the detectors are from the mirror.

When detector  $A$  is placed closer to the mirror, the entanglement profile becomes more sensitive to the presence and trajectories of the mirror. This can be seen from Figure 2, which compares the amount of entanglement that can be harvested around detectors placed respectively near a static mirror and a CW mirror. Putting the mirror even closer, we see from Figure 4 that the mirror “repels” entanglement. More specifically, entanglement harvesting decreases sharply as detector  $B$  approaches the mirror. This is not very surprising since the field operator and hence the Wightman function is designed to

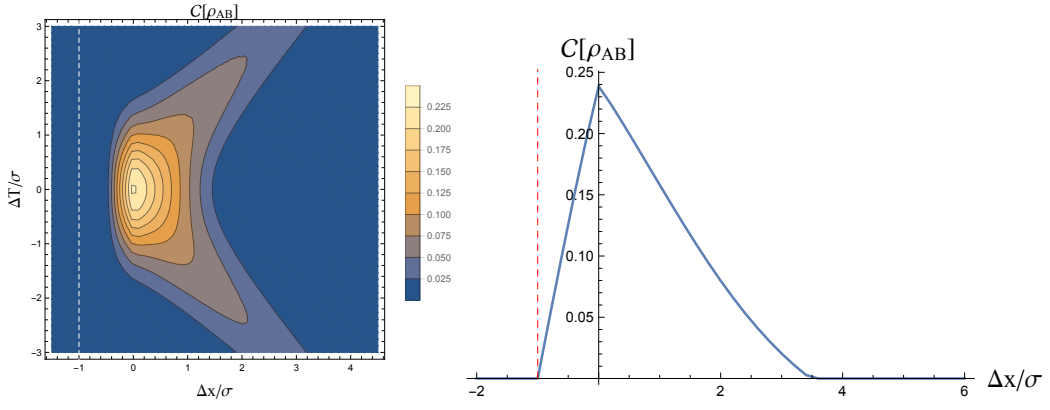


FIG. 4. Entanglement harvesting near a static mirror with  $d_A/\sigma = 1$  and  $\Omega\sigma = 1$ . **Left:** Concurrence contours around detector  $A$ . **Right:**  $t = 0$  cross-section of the plot. Entanglement harvesting clearly drops faster on the mirror side of detector  $A$ , with the red dashed line indicating the mirror's location.

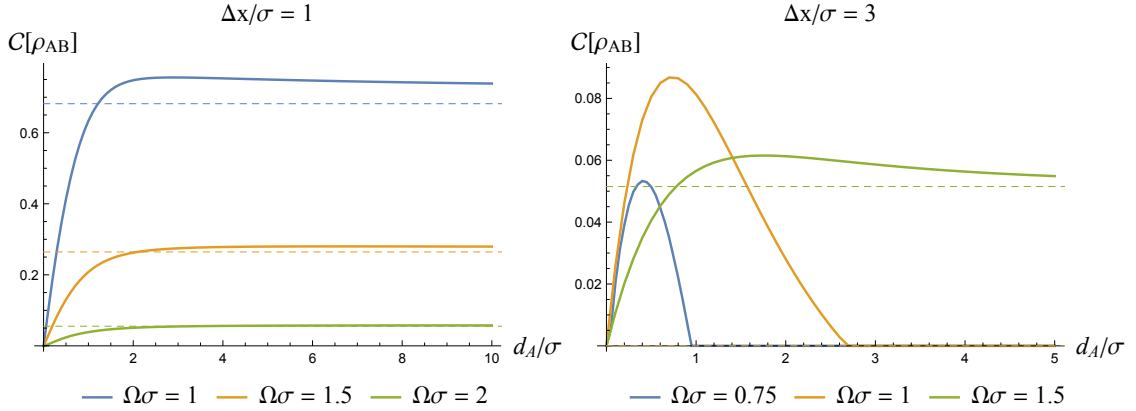


FIG. 5. Concurrence as a function of distance from mirror  $d_A$  with  $\sigma = 1$  and for various energy gaps. The corresponding free space results are shown as dashed lines. We observe entanglement enhancement relative to free-space case in some regions. For the blue and orange curves on the right plot, the free space cases (computed by choosing  $\Lambda = 10^{-12}$ ) have zero concurrence (dotted lines on  $d_A/\sigma$  axis). See section III D for further discussions.

vanish along the mirror trajectory.

It is reassuring that the entanglement profile far from the mirror is similar to the free space case, as illustrated by the similarity between the two cases depicted in Figure 3, as well as their similarity to the flat-space case studied previously (see Figure 1f.2 in [7]). However, the fact that concurrence in presence of a static mirror has a well-defined free space limit is not obvious a priori because of the IR ambiguity for a massless field in  $(1+1)$  dimensions. As we shall see, entanglement harvesting (concurrence) in presence of a mirror in the “far-from-mirror” limit *does not* reduce to the free space value and may eventually fall below it. This is the first instance of entanglement inhibition in mirror spacetime, which we explore in subsequent sections.

Somewhat surprisingly, when we fix the detector separation  $\Delta x$  and allow  $d_A$  to vary instead (moving both detectors closer/farther from the mirror), we find that mirrors can actually *enhance* entanglement for certain parameter choices. For a static mirror this is shown in

Figure 5. The decrease in concurrence close to  $d_A = 0$  is due again to the Dirichlet boundary condition, which happens for all detector separations  $\Delta x$ . For large separations and small gaps (the blue and orange curves in the right figure), concurrence vanishes far from the mirror as we expect. However as the detectors are moved closer to the mirror, concurrence suddenly rises, peaking at some intermediate value before falling off to zero. As the detector separation  $\Delta x$  gets small it becomes easier to harvest entanglement at larger distances, as we expect. Indeed, for very small  $\Delta x$  (left figure), the region of entanglement extraction is very large (possibly everywhere  $d_A > 0$ ). Conversely, we have checked for broad range of parameters, and for sufficiently large  $\Delta x$ , that the concurrence vanishes and so entanglement cannot be extracted anywhere at all.

We also see from Figure 5 that concurrence in the presence of a mirror can overtake the free-space result at large enough  $d_A$  and small enough detector separation. Heuristically, this can be understood as a reflection ef-

fect in which information from one detector can reach the other detector after reflecting off the mirror. The trade off between this reflection effect and the vanishing of the Wightman function close to the mirror leads to a peak in the concurrence at some optimal  $d_A$  away from the mirror. This qualitative behaviour is also present for the other mirror trajectories considered. The main feature displayed here is that of *entanglement enhancement*: mirrors can amplify entanglement relative to the free-space scenario.

## B. CW mirrors

Corresponding results for the CW mirror are shown in Figures 6 and 7. Such mirrors have a constant flux of Hawking radiation. We focus on one particular choice of  $\kappa\sigma = 0.5, \Omega\sigma = 1$ , to keep the analysis simple.

A CW mirror contains more interesting physics compared to its static counterpart. In contrast to the static mirror case, where entanglement vanishes strictly at the mirror due to the boundary condition (cf. Figure 5), we see from Figure 6 that there is a small finite region of *entanglement death* near the mirror. This is reminiscent of the situation when detectors are placed too close to a black hole event horizon [20], but the physics here is clearly different. For the black hole the origin of entanglement death is due to a redshift factor diminishing the non-local correlations relative to the local noise terms. However in the present case there is a (nonlinear) competition between the local noise term  $\sqrt{P_A P_B}$  and the nonlocal term  $|X|$  due to the logarithmic behaviour of the Wightman function. We show in Figure 7 the competition between the nonlocal and local terms corresponding to the left plot to illustrate the point.

CW mirrors can also enhance entanglement. The size of the region of entanglement enhancement depends on the relative separation of the two detectors, as the left plot of Figure 7 shows. Meanwhile, Figure 6 demonstrates that the entanglement structure of this mirror spacetime is not time-symmetric even though the thermal spectrum is time independent; unlike the radiation spectrum, concurrence is sensitive to the non-stationary nature of the spacetime. At “early” times (left plot), in addition to a finite region of entanglement death we observe a finite region of entanglement enhancement relative to the free space result. However, at “late” times (right plot) the size of the entanglement death zone decreases and the harvesting zone always yields an amount of concurrence strictly less than free-space limit. This is likely due to the fact that the mirror velocity is asymptotically null and at  $t = 20$  the mirror is ultrarelativistic. From this we see that generically at late times an accelerating mirror inhibits entanglement compared to early times.

We make a parenthetical remark that while entanglement death near the mirror strictly depends on the non-trivial trajectory of the mirror, entanglement enhance-

ment is a generic feature of mirror spacetimes that occurs for both static and accelerating mirrors. However, Figure 6 shows that entanglement enhancement depends on when we probe the field relative to the motion of the mirror. Since for the CW trajectory the mirror acceleration is not uniform but monotonic, we can conclude that mirror acceleration<sup>3</sup> generically tends to inhibit entanglement relative the corresponding free space situation at late times.

To summarize, we see that the entanglement structure of the CW mirror spacetime is qualitatively different from that of static spacetime: it is mainly characterized by the generic presence of an *entanglement death zone* near the mirror (cf. (a),(b) plots of Figure 6). The strip where this occurs may increase or decrease in size depending on the proximity of the detectors, as shown in Figure 6. The fact that  $\mathcal{C}(\rho_{AB})$  is sensitive to non-stationarity of the mirror also suggests that entanglement is not correlated directly with a thermal flux of radiation, since a CW mirror models a constant flux of Hawking radiation but  $\mathcal{C}(\rho_{AB})$  is clearly dependent on when the detector is switched on.

## C. Black Hole Correspondence Mirrors

While the Carlitz-Willey trajectory models black hole radiation, it does not model black hole collapse because particle creation due to an accelerating mirror following a CW trajectory is *always* thermal [23]. Such a situation corresponds to an eternal black hole that always emits Hawking radiation at the same temperature, i.e. it will need some notion of thermal equilibrium, which typically occurs only on asymptotically anti-de Sitter (AdS) spacetimes (or other spacetimes with some kind of artificial box to enforce equilibrium).

Modelling black hole collapse therefore requires a mirror trajectory in which particle creation is only thermal at late times. In (1+1) dimensions, the analysis is surprisingly manageable and is provided by the mirror trajectory [21, 23]

$$z(t) = v_H - t - \frac{W(2e^{2\kappa(v_H-t)})}{2\kappa} \quad (13)$$

where (to model collapse to a black hole of mass  $M$ ) the identification  $\kappa = 1/4M$  is made and the horizon is given by the future light cone of the point with double-null coordinate  $(v_H, v_0)$  where  $v_H = v_0 - 4M$  [23]. This trajectory has zero velocity and acceleration in the asymptotic past at infinity. It models the shock-wave collapse of a null shell at  $v = v_0$ , i.e. the spacetime that is flat for

<sup>3</sup> We also checked that it is more likely that acceleration, rather than velocity, of the mirror that leads to this suppression of entanglement.

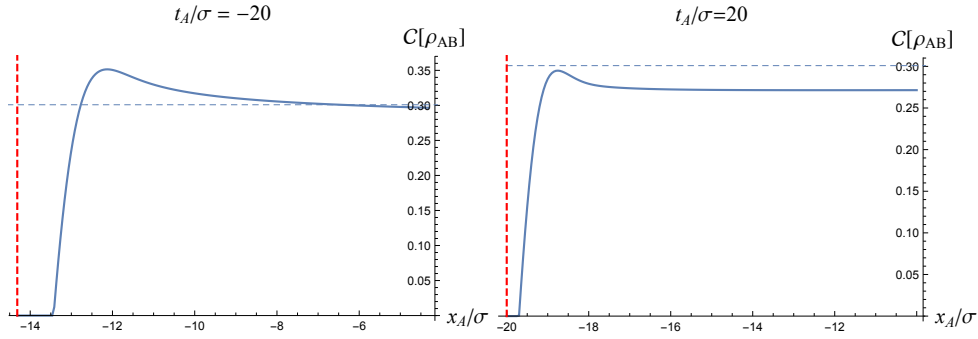


FIG. 6. Concurrence as a function of position of detector  $A$  for various fixed detector separations  $\Delta x$ , with  $\kappa = 0.5, \Omega = 1, \sigma = 1$  for CW mirror (in red at time  $t = t_A = t_B$  when the switching function is peaked). Note that  $x_A/\sigma, \Omega\sigma, \kappa\sigma$  are dimensionless and numerically equal to  $x_A, \kappa, \Omega$  since  $\sigma = 1$ . **Left:**  $t = -20$ . **Right:**  $t = 20$ . The entanglement extracted by the detectors are strictly lower than free space, and in both case there is a finite region near the mirror where entanglement extraction is impossible.

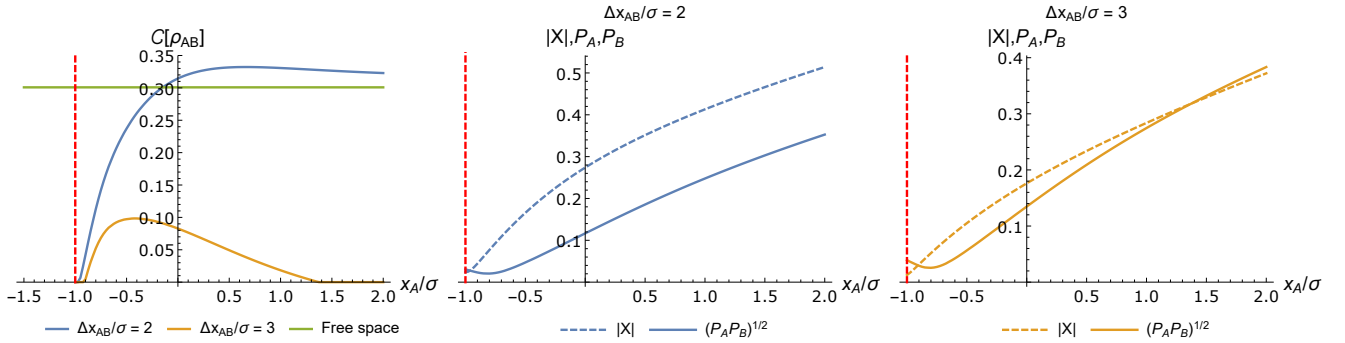


FIG. 7. **Left:** A plot of concurrence for the CW mirror (in red at time  $t = -1$ ), as a function of the position of detector  $A$  for various fixed detector separations  $\Delta x$ , with  $\kappa = 0.5, \Omega = 1, \sigma = 1$ . **Middle:** The nonlocal term  $|X|$  and local noise  $\sqrt{P_A P_B}$  terms for the  $\Delta x = 2\sigma$  trajectory in the left figure. **Right:** The nonlocal term  $|X|$  and local noise  $\sqrt{P_A P_B}$  terms for the  $\Delta x = 3\sigma$  trajectory in the left figure. The small region where the two curves intersect give the small entanglement enhancement region. Note the small zones of entanglement death near the mirror on the left plot for both cases; these appear in the other two plots where we see that  $|X| < \sqrt{P_A P_B}$  very close to the mirror.

$v < v_0$  and Schwarzschild for  $v > v_0$ . We shall call this trajectory the “black hole collapse” (BHC) trajectory.

Since both CW and BHC trajectories are asymptotically null in the future, we might expect that their differences must arise at early and intermediate times. The parameter  $v_H$  in the ray-tracing function (12) determines which null ray the mirror asymptotically approaches. Thus it provides a degree of freedom in choosing the location of the horizon. The parameter  $\kappa$  is an effective acceleration parameter that is inversely proportional to the mass of the black hole. Unlike the CW trajectory, the mirror is at  $x = \infty$  when  $t = -\infty$  whereas the CW mirror is at  $x = -\infty$ , i.e. the CW mirror attains zero velocity midway (see Figure 1). As such, for the BHC trajectory, in principle the mirror will cross the detectors at some time; in this case, we imagine that the detectors have Gaussian switching that effectively makes the detector active only when the mirror is on the left side of both detectors and imposes the boundary condition so that the field vanishes on the left side of the mirror.

We are primarily interested in the generic behaviour of entanglement between the detectors as compared to the static and CW mirror cases. First, we see that a BHC mirror reproduces the static mirror limit, as expected when the detectors are very far away from the BHC mirror for a given fixed value of  $\kappa, v_H$ ; the results are similar to that of Figure 3 and we have not illustrated them here. Next, for fixed detector separation  $\Delta x$ , we find that concurrence changes as function of the distance of the closer detector  $d_A$  from the mirror (at the time the switching function peaks). For two extreme cases, we obtain expected results (not illustrated) generic to all three mirror trajectories: if the detectors are very close, we find that we can extract entanglement from the vacuum very far away from the mirror; if the detectors are very widely separated, no entanglement can be extracted at all for any  $d_A$ .

The situation becomes more interesting when we choose to turn on the detectors at different times, to see what “early” or “late” times do to the concurrence. Un-



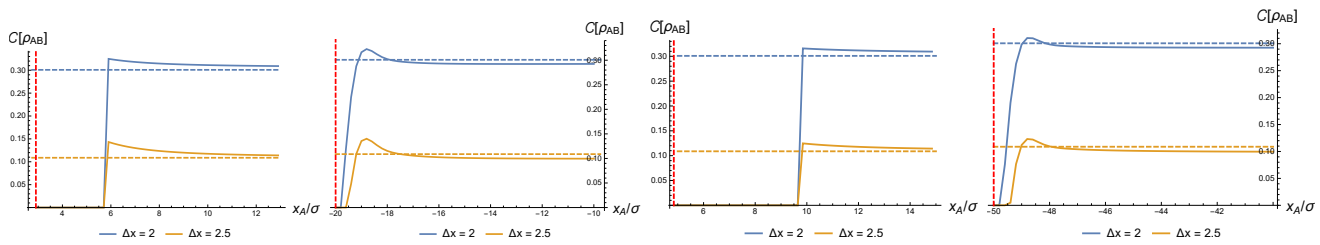


FIG. 8. Concurrence for a BHC mirror (in red at time  $t$  when the detector is temporally peaked) for various fixed detector separations as a function of position of detector  $A$  with  $\kappa = 0.25, \Omega = 1, \sigma = 1$ . From left to right: (a)  $v_H = 0$ , the “early” time  $t = -20$ . (b)  $v_H = 0$ , the “late” time  $t = 20$ . (c)  $v_H = 50$ ,  $t = 0$ . (d)  $v_H = -50$ ,  $t = 0$ . In these plots  $x_A$  denotes the  $x$  coordinate of detector  $A$  in standard Minkowski coordinates, hence distance to the right of the mirror is  $d_A = |x_{\text{mirror}} - x_A|$ , with  $x_{\text{mirror}}$  is given by the red line.

like the CW trajectory, the BHC mirror trajectory has no turning point, i.e. it always moves in the negative  $x$  direction, and so it is not obvious what will happen here. The results are illustrated in Figure 8, and turn out to be qualitatively similar to the CW trajectory. We have an entanglement death zone near the mirror as well as entanglement enhancement further away; this is particularly clear upon comparing plots (a) and (b) in Figure 8. There is a quantitative difference: the death zone is much wider than in the CW scenario. The “early” and “late” time behavior by time-shift of the detector switching time are not symmetric due to the nature of the trajectory, which is expected of black hole collapse models, and this asymmetry is much more apparent than in the CW case. The radically shrinking width of the death zone from early (a) to late (b) times is likely due to the differing magnitudes of the mirror velocity. This difference is much greater for the BHC trajectory than for the CW trajectory. The overall entanglement inhibition at late times, however, is a generic feature of accelerating mirror spacetimes.

We can also inquire as to what happens if we shift the position of the horizon, say to  $v_H = \pm 50$ . From (13), we can see that this simply corresponds to shifting the trajectory (Figure 1) upwards or downwards in time by the corresponding amount. Hence, for example, setting  $v_H = 50$  and  $t = 0$  is equivalent to  $v_H = 0$ ,  $t = -50$ . Physically, the value of  $v_H$  influences at which null coordinate the mirror asymptotically approaches null velocity. We can think of  $v_H = 50$  as the case when the horizon forms “late”, since at the time the detector is turned on its velocity is far from ultra-relativistic; likewise for  $v_H = -50$  the horizon forms “early”. In the latter case the detector sees the mirror already at ultra-relativistic speed. The results are shown in diagrams (c) and (d) in Figure 8. The similarity with diagrams (a) and (b) is striking, justifying the interpretation as early/late horizon formation. We find the same qualitative result as that of CW trajectory, namely entanglement death near the mirror, generic entanglement enhancement in some regimes especially at early times, and overall entanglement inhibition (relative to free space) at late times.

The main contrast between the CW and BHC trajec-

tories seem to come from the large width of the entanglement death zone at early times, while at late times diagrams (c) and (d) in Figure 8 are strikingly similar to the respective left and right diagrams in Figure 6. This can be traced to the fact that the BHC trajectory is unidirectional whilst the CW trajectory changes direction at  $t = -(2\kappa)^{-1}$ . Since in both cases proper acceleration is small at early and late times and only significant at some intermediate times, this distinction is likely to be due to the difference in the velocity and position (which has a turning point for CW but not BHC) during time evolution. In this sense, entanglement harvesting can be used to distinguish between a collapsing spacetime and an eternal black hole spacetime (corresponding respectively to BHC and CW trajectories) if we were to take seriously the correspondence between these mirror spacetimes and (1+1) dimensional black hole spacetimes as argued in [16, 17, 21, 23].

#### D. Detector Response and Concurrence in the presence of a boundary

One peculiarity we found in this work is that in (1+1) dimensions, there seems to be a slow but unbounded growth of the transition probability  $P(\Omega)$  as a function of distance from the boundary, which we denote by  $d$ . In particular, this means that in (1+1) dimensions the static mirror does not smoothly recover the free space limit as  $d \rightarrow \infty$ , which is in contrast to the expectation that a detector does not sense nonlocal differences and in particular whether there is a boundary far away. This may influence the reliability of entanglement measures that inherently depend on  $|X|$  and  $P(\Omega)$ . Although the problem of particle detectors in half-space has been previously considered [12, 13, 24], the growth of  $P(\Omega)$  as a function of  $d$  was not clarified. We will compare two scenarios for static Dirichlet boundary conditions in (1+1) and (3+1) dimensions. We will show that the peculiarity is dimension dependent and not generically true in the presence of a boundary.

In (3+1) dimensions, the Wightman function for a Dirichlet boundary on the  $yz$ -plane such that a detector



is located at  $(d, 0, 0)$  where  $d > 0$  is given by the image sum

$$W(x, x') = \frac{-1}{4\pi^2} \left[ \frac{1}{(\Delta\tau - i\epsilon)^2} - \frac{1}{(\Delta\tau - i\epsilon)^2 - 4d^2} \right] \quad (14)$$

where the second term is the image term that gives the distance dependence  $d$ . Evaluating the expression for  $P(\Omega)$  in Eq. (6) for this Wightman function and the usual Gaussian switching in Eq. (7), we will get two contributions to the integral:

$$P(\Omega) = P_{\text{free}}(\Omega) + P_{\text{image}}(\Omega) \quad (15)$$

where

$$P_{\text{free}}(\Omega) = -\frac{\sigma}{\sqrt{16\pi^3}} \int_{-\infty}^{\infty} dy \frac{e^{-\frac{y^2}{4\sigma^2}} e^{-i\Omega y}}{(y - i\epsilon)^2}, \quad (16)$$

$$P_{\text{image}}(\Omega) = \frac{\sigma}{\sqrt{16\pi^3}} \int_{-\infty}^{\infty} dy \frac{e^{-\frac{y^2}{4\sigma^2}} e^{-i\Omega y}}{(y - i\epsilon)^2 - 4d^2}.$$

The first term is just the finite-time response of a detector in free space and hence is independent of  $d$ . The image term [25] is known to be finite even in free space for finite width  $\sigma > 0$ . We are interested in the behaviour of the integral of the image term as  $d$  increases, which we show in Figure 9. This is in fact not hard to see from the form of the Wightman function: as  $d \rightarrow \infty$ , the image term becomes more and more negligible because the finite

width Gaussian window suppresses contributions at large  $u$ . Hence, in  $(3+1)$  dimensions the phenomenology of inertial (static) detectors in Minkowski half-space has the expected free-space limit as  $d \rightarrow \infty$ .

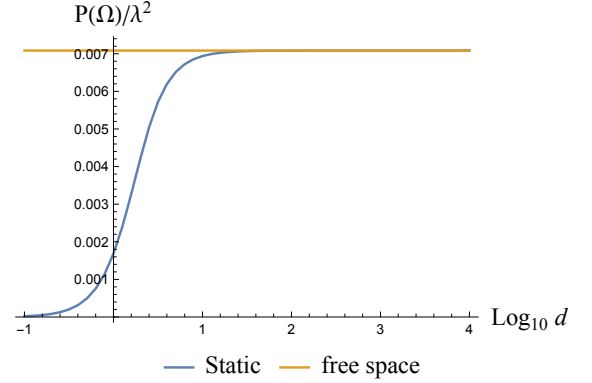


FIG. 9. Transition probability for Gaussian switching  $\sigma = 1$  and  $\Omega = 1$  ( $\Omega\sigma = 1$ ) in  $(3+1)D$ . Near the mirror  $P(\Omega)$  decays quickly, and far from the mirror the contribution from the image term vanishes quickly. In this figure the asymptotic behaviour is reached at  $d/\sigma \sim 10^2$ .

This, however, is not true in  $(1+1)$  dimensions because the Wightman function has a logarithmic instead of power law dependence on  $d$ . For a static mirror, the expression is instead

$$P_{\text{free}}(\Omega) = -\frac{\sigma}{\sqrt{16\pi^3}} \int_{-\infty}^{\infty} dy e^{-i\Omega y} e^{-\frac{y^2}{4\sigma^2}} \log \left[ \frac{(y - i\epsilon)^2}{\Lambda^2} \right]$$

$$P_{\text{image}}(\Omega) = \frac{\sigma}{\sqrt{16\pi^3}} \int_{-\infty}^{\infty} dy e^{-i\Omega y} e^{-\frac{y^2}{4\sigma^2}} \log \left[ \frac{|(y - i\epsilon)^2 - 4d^2|}{\Lambda^2} \right] \quad (17)$$

where we have made the free-space IR cutoff  $\Lambda$  explicit for comparison. Recall that in  $(1+1)$  dimensions, there is an IR ambiguity: the cutoff  $\Lambda$  renders  $P(\Omega)$  ambiguous up to an arbitrary constant. This means that for a massless field we cannot quite naively take free space as a reference point. However this ambiguity is at present unimportant, because the image term in the Wightman function (the denominator of the logarithm) *cannot* be made to vanish as  $d \rightarrow \infty$  and in fact it becomes dominant at large  $d$ . The comparison is shown in Figure 10.

What this highlights is that within perturbation theory, one should take extra care in distinguishing what is due to the physics of the boundary and what is an artifact of the dimensionality of spacetime. An effect strictly confined to  $(1+1)$  dimensions will not necessarily provide guidance to our understanding of  $(3+1)$  dimensional physics. In particular the observable  $P(\Omega)$  in the presence of a mirror is generically an ill-behaved quantity in  $(1+1)$  dimensions, even without the IR ambiguity asso-

ciated with the free-space counterpart.

However, not all is lost. As we saw earlier, the concurrence is a quantity based on the *difference*  $|X| - \sqrt{P_A P_B}$ . Roughly speaking, we can understand this by noting that for static mirror we have a  $\log[(\Delta\tau - i\epsilon)^2 - 4d_A^2]$  dependence due to the form of the Wightman  $W(x_A, x'_A)$ . Very roughly, for  $|X|$  we will have a contribution of the form

$$W(x_A, x'_B) \sim \log [((\Delta\tau - i\epsilon) - (2d_A - \Delta x_{AB}))^2] \quad (18)$$

which can be seen to scale the same way as  $\sqrt{P_A P_B}$  for any fixed  $x_{AB}$ . From this, we expect that concurrence  $\mathcal{C}$  is in some sense ‘dimension-independent’: it removes the part of the Wightman function that depends on the *absolute distance*  $d_A, d_B$  away from the mirror. What remains is the *relative distance* dependence  $\Delta x_{AB}$  of  $\mathcal{C}(\rho_{AB})$  which leads to the usual decay of correlations as we make the detectors have larger spacelike separation.

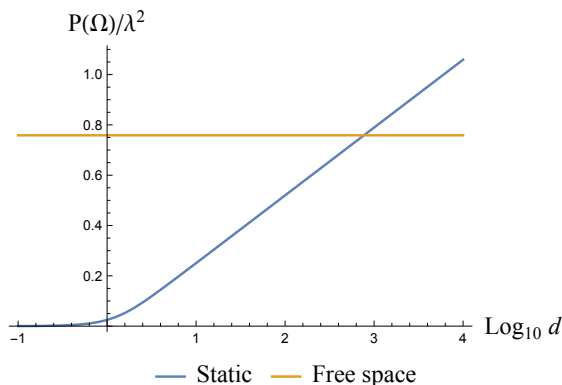


FIG. 10. Transition probability for Gaussian switching  $\sigma = 1$  and  $\Omega = 1$  ( $\Omega\sigma = 1$ ) in  $(1+1)$  dimensions. Near the mirror  $P(\Omega)$  still decays quickly, but far from the mirror the contribution from the image term dominates and will exceed the free space case for any choice of IR cutoff  $\Lambda$ .

Effectively,  $\mathcal{C}(\rho_{AB})$  ‘regularizes’ the ill-behaved part of  $|X|$  and  $P(\Omega)$  somewhat analogous to adding counterterms in QFT. This provides strong evidence that we can rely on concurrence calculations in  $(1+1)$  dimensions even if we cannot separately trust the entries in the evolved density matrix  $\rho_{AB}$  as  $d \rightarrow \infty$  due to the divergent behavior at large mirror distance.

With some thought, this growth of  $P$  with distance from the mirror  $d$  may not be as surprising as it seems: it is already known in classical gravity that the Newtonian gravitational potential in one-dimensional space also grows linearly with separation between masses [26, 27] unlike the  $1/r$  power law in the three-dimensional context [28]. We should also remark that since this is an inherent problem associated with the long-distance behaviour of the Wightman function, the issue will not disappear for general choices of ray-tracing functions. We can check this numerically for the three ray tracing functions in this paper – we find that indeed  $\mathcal{C}(\rho_{AB})$  seems to provide proper regularization in  $(1+1)$  dimensions: that is, for each ray tracing function we find similar divergences in both the nonlocal term  $|X|$  and probability  $P$ , but not in  $\mathcal{C}(\rho_{AB})$ .

As a consequence of this ‘regularization’, the concurrence  $\mathcal{C}(\rho_{AB})$  also does not suffer from an IR ambiguity even in free space. For the same reason as why the divergences in the  $d_A \rightarrow \infty$  limit is subtracted off by the definition of  $\mathcal{C}(\rho_{AB})$ , the IR ambiguity is also subtracted off. We can thus think of  $\mathcal{C}(\rho_{AB})$  as having an IR regulator *by definition*. This is the reason why the free space limit of the concurrence in the presence of mirrors is well-defined (cf. Figure 5). Since concurrence is IR-regular, it can be reverse-engineered to induce a natural IR cutoff for the free-space Wightman function. This is shown in Figure 11. We see that the concurrence approaches an approximately constant value once  $\Lambda$  is reasonably small, which we can take to be at least  $\Lambda \lesssim 10^{-3}$ . In [7] and [22] the value  $\Lambda = 10^{-3}$  were adopted arbitrarily due to the

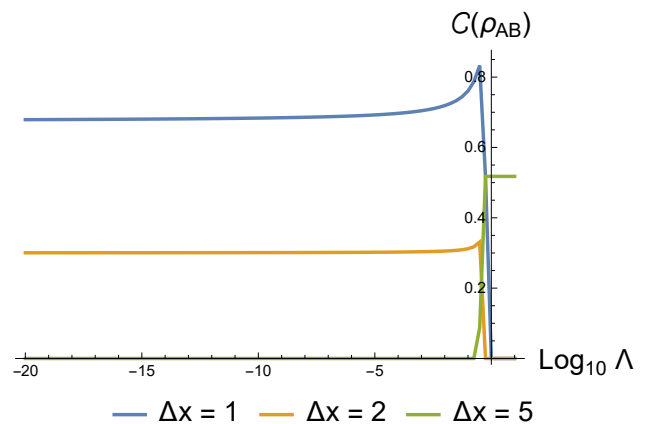


FIG. 11. The concurrence in free space as a function of IR cutoff (in logarithmic scale), for  $\Omega = 1$  and  $\sigma = 1$  in natural units (i.e.  $\Omega\sigma = 1$  is dimensionless).

ambiguity argument: this value is arguably small enough for their purposes, though choosing a smaller value allowed by the numerical precision used during computation is preferable. We verified this for up to  $\Lambda \sim 10^{-100}$  and the IR ambiguity does not seem to play a role in computation of  $\mathcal{C}(\rho_{AB})$ .

In short, we can think of concurrence  $\mathcal{C}(\rho_{AB})$  as a naturally ‘regularized’ quantity for a massless scalar field in all dimensions, unlike the IR-divergent  $|X|$ ,  $P$  in  $(1+1)$  dimensions. Furthermore, the regularity of  $\mathcal{C}(\rho_{AB})$  may be instead used to induce a natural IR cutoff  $\Lambda$  for the detector joint density matrix  $\rho_{AB}$ .

#### IV. CONCLUSION

We have performed in  $(1+1)$  dimensions the first investigation of entanglement harvesting between two detectors in the presence of mirrors with both static and non-inertial trajectories, focusing on the CW and BHC trajectories for the latter because of their respective correspondence to eternal black holes and black hole formation. We find that a similar correspondence exists for their entanglement structures, in particular the phenomenon of an entanglement death zone, similar to that recently found for a black hole event horizon [20]. We also found heuristically and numerically that concurrence  $\mathcal{C}(\rho_{AB})$  is naturally ‘regularized’ in  $(1+1)$  dimensions. Therefore, the IR ambiguity that plagues each entry of the detector density matrix  $\rho_{AB}$  does not affect  $\mathcal{C}(\rho_{AB})$ ; furthermore, it seems possible to choose a natural, reasonably small IR cutoff using concurrence since  $\mathcal{C}(\rho_{AB})$  converges to a fixed value for sufficiently small  $\Lambda$ .

We also find that there are differences between the entanglement extraction behaviour of CW and BHC mirror spacetimes, providing strong evidence that UdW detectors can distinguish between a collapsing black hole spacetime and an eternal black hole spacetime depend-

ing on when they are switched on (late or early). While this does not mean that mirror spacetimes is the same as black hole spacetime, it reinforces the fact that one can map the aspects of black hole physics to that of moving mirrors, effectively mapping the Unruh and Hawking effects into the dynamical Casimir effect. This suggests the possibility of simulating such effects in the laboratory.

Finally, and perhaps most interestingly, we also find that mirrors can enhance entanglement: entanglement harvested between two detectors can be greater in the presence of a mirror as compared to free space. Qualitatively this enhancement is largely trajectory-independent, and is thus attributable to the inherent presence of a Dirichlet boundary condition. Quantitatively there are distinctions between different mirror trajectories, as a comparison between Figures 5 and 6 indicates. We focused on three types of mirror trajectories that have the simplicity of having smooth ray-tracing functions  $p_j(u)$  that are regular for all  $u \in \mathbb{R}$ . Import-

tant trajectories such as a mirror with constant uniform acceleration have ray-tracing functions that are not defined for all  $u$ , indicating that only some modes at future null infinity  $\mathcal{I}^+$  can be ‘ray-traced’ to modes at past null infinity  $\mathcal{I}^-$ . We have also not investigated the case of piecewise mirror trajectories, such as a mirror that only accelerates at  $t = 0$  and static at  $t \leq 0$ , which are often used in analyses involving Bogoliubov transformations. We defer this for future work.

## V. ACKNOWLEDGMENT

This work was supported in part by the Natural Sciences Engineering Research Council. Erickson Tjoa thanks Eduardo Martín-Martínez and Robie A. Hennigar for helpful discussions.

- 
- [1] L. Bombelli, R. K. Koul, J. Lee, and R. D. Sorkin, Phys. Rev. D **34**, 373 (1986).
  - [2] M. Srednicki, Phys. Rev. Lett. **71**, 666 (1993).
  - [3] S. Ryu and T. Takayanagi, Phys. Rev. Lett. **96**, 181602 (2006).
  - [4] S. J. Summers and R. Werner, Physics Letters A **110**, 257 (1985).
  - [5] A. Valentini, Physics Letters A **153**, 321 (1991).
  - [6] G. Salton, R. B. Mann, and N. C. Menicucci, New J. Phys. **17**, 035001 (2015).
  - [7] A. Pozas-Kerstjens and E. Martín-Martínez, Phys. Rev. D **92**, 064042 (2015).
  - [8] E. Martín-Martínez, A. R. H. Smith, and D. R. Terno, Phys. Rev. D **93**, 044001 (2016).
  - [9] G. V. Steeg and N. C. Menicucci, Phys. Rev. D **79**, 044027 (2009).
  - [10] C. M. Wilson, G. Johansson, A. Pourkabirian, M. Simoen, J. R. Johansson, D. T., F. Nori, and P. Delsing, Nature **479**, 376 (2011).
  - [11] N. Birrell and P. Davies, *Quantum Fields in Curved Space*, Cambridge Monographs on Mathematical Physics (Cambridge University Press, 1984).
  - [12] N. Suzuki, Classical and Quantum Gravity **14**, 3149 (1997).
  - [13] P. C. W. Davies, Z. X. Liu, and A. C. Ottewill, Classical and Quantum Gravity **6**, 1041 (1989).
  - [14] L. Hodgkinson, *Particle detectors in curved spacetime quantum field theory*, Ph.D. thesis (2013).
  - [15] R. D. Carlitz and R. S. Willey, Phys. Rev. D **36**, 2327 (1987).
  - [16] M. R. R. Good, P. R. Anderson, and C. R. Evans, Phys. Rev. D **88**, 025023 (2013).
  - [17] M. R. R. Good, P. R. Anderson, and C. R. Evans, Phys. Rev. D **94**, 065010 (2016).
  - [18] M. R. R. Good, K. Yelshibekov, and Y. C. Ong, Journal of High Energy Physics **2017**, 13 (2017).
  - [19] M. R. R. Good and E. V. Linder, Phys. Rev. D **97**, 065006 (2018).
  - [20] L. J. Henderson, R. A. Hennigar, R. B. Mann, A. R. H. Smith, and J. Zhang, (2017).
  - [21] P. R. Anderson, M. R. R. Good, and C. R. Evans, “Black hole - moving mirror i: An exact correspondence,” in *The Fourteenth Marcel Grossmann Meeting*, pp. 1701–1704.
  - [22] E. Martín-Martínez and J. Louko, Phys. Rev. Lett. **115**, 031301 (2015).
  - [23] M. R. R. Good, P. R. Anderson, and C. R. Evans, “Black hole - moving mirror ii: Particle creation,” in *The Fourteenth Marcel Grossmann Meeting*, pp. 1705–1708.
  - [24] E. G. Brown and J. Louko, JHEP **08**, 061 (2015), arXiv:1504.05269 [hep-th].
  - [25] L. Sriramkumar and T. Padmanabhan, Classical and Quantum Gravity **13**, 2061 (1996).
  - [26] R. B. Mann and S. F. Ross, Class. Quant. Grav. **10**, 1405 (1993), arXiv:gr-qc/9208004 [gr-qc].
  - [27] T. Ohta and R. B. Mann, Class. Quant. Grav. **13**, 2585 (1996), arXiv:gr-qc/9605004 [gr-qc].
  - [28] C. Romero and F. Dahia, International Journal of Theoretical Physics **33**, 2091 (1994).